A flow-based microfluidic device for spatially quantifying intracellular calcium ion activity during cellular electrotaxis

View Online   Export Citation   CrossMark

Joshua Cole[1,a)] (iD) and Zachary Gagnon[2,b)] (iD)

AFFILIATIONS

[1]Department of Chemical and Biomolecular Engineering, Johns Hopkins University, Baltimore, Maryland 21218, USA
[2]Department of Chemical Engineering, Texas A&M University, 203 Jack E. Brown Building, College Station, Texas 77843, USA

Note: This article is part of the special topic, Festschrift for Professor Hsueh-Chia Chang.
[a)]jcole35@jhu.edu
[b)]zgagnon@tamu.edu

ABSTRACT

How a cell senses, responds, and moves toward, or away from an external cue is central to many biological and medical phenomena including morphogenesis, immune response, and cancer metastasis. Many eukaryotic cells have internal sensory mechanisms that allow them to sense these cues, often in the form of gradients of chemoattractant, voltage, or mechanical stress, and bias their motion in a specific direction. In this study, a new method for using microfluidics to study the electrotactic migration of cells is presented. Electrotaxis (also known as galvanotaxis) is the phenomenon by which cells bias their motion directionally in response to an externally applied electrical field. In this work, we present a new flow-based, salt bridge-free microfluidic device for imaging and quantifying cell motility and intracellular ion activity during electrotaxis. To eliminate salt bridges, we used a low nanoliter flow rate to slowly drive Faradaic waste products away from and out of the electrotaxis zone. This cell migration zone consisted of an array of fluidic confinement channels approximately $2\,\mu m$ in thickness. This confined height served to insulate the migrating cells from the electric field at the top and bottom of the cell, such that only the two-dimensional perimeter of the cells interacted with the electrical source. We demonstrate the ability to quantify the electrotactic velocity of migrating *Dictyostelium discoideum* cells and show how this confined design facilitates the imaging and quantification of the ion activity of electrotaxing cells. Finally, by spatially imaging the calcium concentration within these cells, we demonstrate that intracellular calcium preferentially translocates to the leading edge of migrating *Dictyostelium* cells during electrotaxis but does not exhibit this behavior during migration by chemotaxis in a gradient of cyclic adenosine 3′,5′-monophosphate or when cells freely migrate in the absence of an external cue.

INTRODUCTION

Electrotaxis (also known as galvanotaxis) is the phenomenon by which cells bias their motion directionally in response to an externally applied electrical field.[1] Since electrotaxis of living cells was first discovered over a century ago, motile cells including neurons, fibroblasts, lymphocytes, leukocytes, macrophages, neural crest cells, cancer cells, and slime molds have shown the ability to detect gradients in electrical potential (voltage) and display directional migration toward the negative (cathode) or positive (anode) charged electrode depending on the cell type and growth conditions.[2] Electrotaxis has been shown to be important in a number of cellular processes including embryogenesis, cancer cell migration, wound healing, and angiogenesis.[3] Ionic currents have been detected around large single cells including developing eggs and pollen tubes and suggested as a cue to help drive spatial organization for division or growth. Furthermore, electric fields can be used to direct the polarity in many cell types including bacteria, neutrophils, and fungi.

Unlike chemotaxis[4,5] however, very little is known in terms of the underlying physical mechanism of how electrical cues are transduced to influence the cytoskeletal organization for polarity and motility, and it is unknown why a cell chooses to migrate in one particular direction or another. Corneal endothelial cells and human metastatic breast cancer cells, for example, tend to move

toward the anode of an electric field,[6,7] whereas rat prostate cancer cells, epithelial cells, and *Dictyostelium discoideum*[8–10] move toward the cathode. The influx and release of calcium ions has been shown to be heavily associated with cell migration and to play an important role during electrotaxis.[7,11,12] However, the influx and intracellular translocation of these ions and the resulting intracellular concentration profiles have been traditionally difficult to study within electrotaxing cells. In particular, intracellular calcium ions have been demonstrated to be required for the electrotaxis of *Dictyostelium* cells,[12] and it is generally believed that electrotaxis initiation occurs at the cell membrane due to a field-induced ion flux across the membrane,[13] but more detailed dynamics and intracellular distribution of this ion activity remains unknown. One reason for this lack in understanding is due to a lack of an experimental setup capable of investigating local distributions of ions and their transport at the single cell level during cellular electrotaxis.

As traditional electrotaxis experiments have been largely performed on flat, open substrates such as Petri dishes or glass coverslips,[2,14] the electric field can be nonuniform, and the apparatus can be bulky and lack reproducibility. To improve repeatability and precise control over the electric field strength, the use of microfluidic devices to study electrotaxis has become increasingly popular over the last decade. One of the main benefits of microfluidics is that cells can be loaded into a controlled fluidic environment with well-defined and uniform electric fields. However, many microfluidic devices are still difficult to fabricate and can require complicated multilayer device construction and/or salt bridges to prevent contamination by reactions at the electric field-producing electrodes.[5,14,15] In this work, we present a new microfluidic flow-based electrotaxis/chemotaxis device for studying ion transport in electrotaxing cells and demonstrate its use in quantifying the distribution of intracellular calcium within single electrotaxing *D. discoideum* cells. Moreover, we demonstrate that calcium ion translocation during electrotaxis is distinctly different when compared to the calcium ion activity in these same cells during chemotaxis or in the absence of an external chemical or electrical cue.

CELLS AND PREPARATION

Due to their ease in maintenance, their quick movement and response times, their general use in motility studies, and the amount of previous knowledge over their electrotactic behavior, *Dictyostelium* is a prime cell line to start studying the physiological mechanisms by which electrotaxis occurs.[10,16,17] Cells were derived from the axenic strain Ax2 of *D. discoideum*. Cells were grown in 1.5× HL-5 medium with glucose (FORMEDIUM Ltd.) (1 l H_2O, 15 g Bacto-Proteose Peptone, 3.9 g yeast extract, 3.0 g glucose, 0.13 g $Na_2HPO_4 \cdot 7H_2O$, 0.13 g KH_2PO_4). When starved, *Dictyostelium* cells undergo a developmental process where signaling proteins are upregulated, and after a few hours, they develop a polarized morphology as well as the ability to sense and chemotax toward sources of cyclic adenosine $3',5'$-monophosphate (cAMP). When exponentially growing cells reached a concentration of $2–4 \times 10^6$ cells/ml, cells were washed in the development buffer free of nutrients (DB; 5 mM $KHPO_4$, 5 mM Na_2HPO_4, 1 mM $MgCl_2$, 0.2 mM $CaCl_2$, pH = 6.4) and resuspended at a concentration of 2×10^7 cells/ml. Cell were then starved in DB: a 2 ml volume of

cells in DB was shaken for 4 h at 180 rpm and a 100 μl pulse of a 2 μM cAMP solution in DB was added every 6 min after the first hour. All experiments and cell preparation was performed at 22 °C, and all cell migration experiments were performed in a solution of DB with 7.5 μM cAMP (except chemotaxis experiments where a gradient of cAMP is required). Experiments involving chemotaxis were performed by pumping a solution of DB + cAMP into one side flow channel to produce a linear chemical gradient of 20 nM/μm across the cell chambers.

MICROFLUIDIC DEVICE FOR DIRECT, CONTROLLED, AND UNCONTAMINATED ELECTROTAXIS

Experiments were performed using microfluidic devices constructed of polydimethylsiloxane (PDMS; Momentive, RTV 615A) using standard soft lithographic fabrication methods.[18] Briefly, a 1:10 mixture of PDMS elastomer and curing agent was poured atop a lithographically fabricated polymer mold, cured, and gently peeled off. Fluid ports were punched into the PDMS using a 0.75 mm biopsy punch (Ted Pella Inc.), and the microfluidic device and coverslip were exposed to oxygen plasma (Jelight, Model 42A) and immediately aligned and sealed under an inverted microscope, and the assembled device was baked at 90 °C for 2 h to ensure strong bonding.

The microfluidic geometry is constructed of two different channel heights, a "tall" (80 μm) set of channels used largely for flow control and a "shallow" (2.3 μm) set of channels designed for cell electrotaxis experiments. After plasma treating the wafer for 5 min at 100 W (Technics West Inc., PE II-A Plasma System), the "shallow" confinement channels were patterned on a silicon wafer (Wafer World Inc., SKU: 2886) using a low viscosity photoresist (MicroChem, SU-8 2002). A second "thick" photoresist (MicroChem, SU-8 3050) was spin-coated onto the wafer and patterned to create nonconfining side channels and cell-seeding chambers. Lithography of both channel heights was performed following MicroChem's processing guidelines for each specific product. The final device consisted of confining electrotaxis cell channels orthogonally aligned with two larger main side channels. The cell channels were designed with a length L = 150 μm and a width W = 50 μm, with a microchannel height of 2.3 μm (Fig. 1). A more detailed micrograph of the confinement cell chambers is shown in Fig. 1(c). These shallow channels served to electrically confine the top and bottom of the cells during migration to insulate these regions from the electric field. To eliminate the possibility of these shallow channels collapsing, we integrated a pair of supportive pillars at each confined channel inlet and channel outlet. The pillars formed from PDMS did not impede cell invasion or impact the formation of the passive gradient or the electric field [Fig. 2(a)].

The confinement channels serve two important purposes in this work. First, the insulating nature of the PDMS and glass surfaces prevent the electric field from interacting with the top and bottom of each cell. This feature restricts the electric field interaction at the cell membrane to the sides, specifically looking at the front and back of the cells where the voltage differential is the greatest. Experimentally, this allows us to focus our efforts and analysis on the cell perimeter. Further, the effects of cellular confinement serve to keep the cell in a state that increases the degree of surface area for the visual study under confocal microscopy.
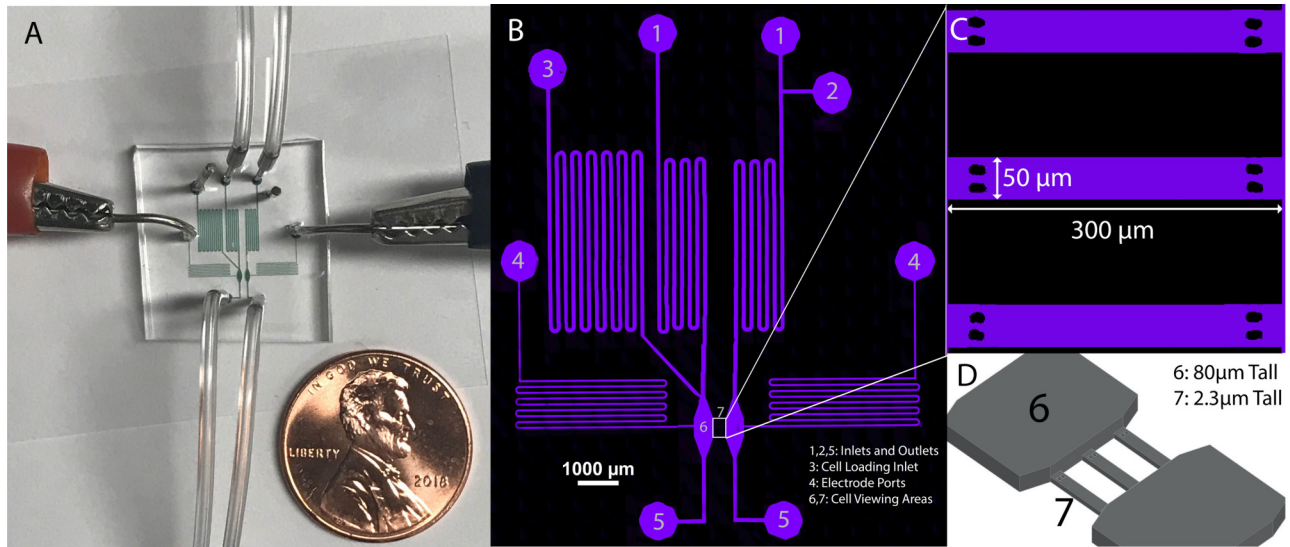
FIG. 1. (a) Electrotaxis device showing fluid inlets, outlets, and electrotaxis electrodes. Channels filled with a colorimetric dye for imaging and penny shown for scale. (b) Confocal image of microfluidic channels filled with fluorescent dye Alexa Fluor 647 and labeled: 1. Standard buffer inlets, 2. Optional inlet for buffer switching, as might be useful for chemotaxis experiments, 3. Cell loading inlet, 4. Electrode ports, 5. Outlets, 6. 80 μm tall channel for cell seeding, 7. 2.3 μm tall constrictive channels for cell viewing during experimentation. (c) Zoomed in view of the three constrictive channels located in section 7. (d) 3D illustration of cell channels to depict height difference between section 7 and the main flow and cell loading channels. A micrograph of this region is shown in Fig. 2(b).

As can be seen in Fig. 1(a), the electrotaxis microfluidic device is a relatively simple structure, consisting of a single layer of PDMS bonded to a glass coverslip. Because of our flow-based design, this setup requires no salt bridges, which can often complicate a microfluidic design. Fluid inlets were utilized to deliver a controlled flow of the cell buffer into the device and to wash out any potential damaging Faradaic reaction products. To deliver the electric field, thin 30 AWG platinum-rhodium wires (Omega, SPPL-010) were inserted into the two separate side ports of the chip, and a voltage is delivered across these ports using a linear direct current (DC) power supply (Circuit Specialists, CSI12001X). These thin (~250 μm diameter) wires were chosen as we observed a decrease in Faradaic reactions with a decrease in wire diameter. Shown in Fig. 1(b), during the normal operation, the buffer flowed from Inlet 1, through Cell Area 6, to Outlet 5 on each side, respectively, at a flow rate of 16 μl/min on each side, using pressure driven flow delivered with a microfluidic flow controller (Elveflow OB1 Pressure Controller). Inlet 2 can also be used if experimentation
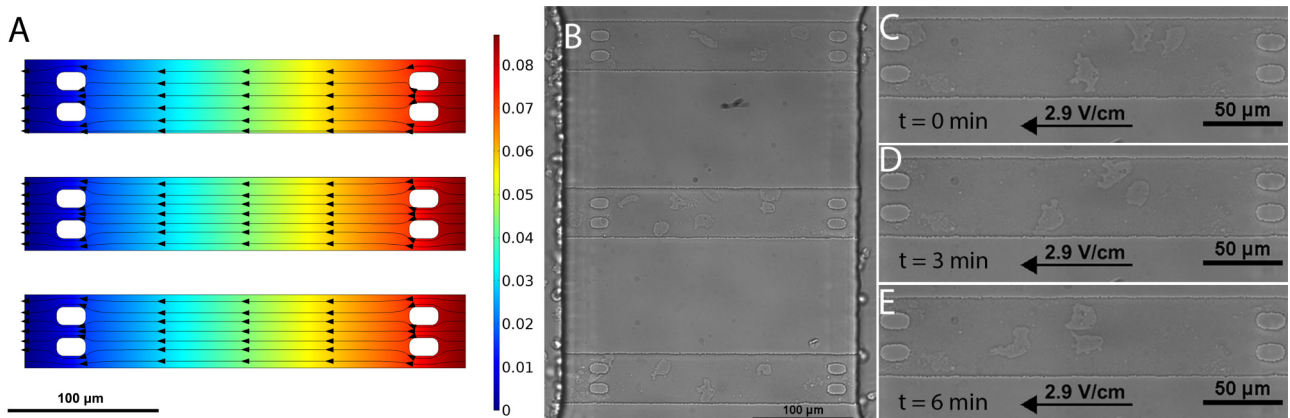
FIG. 2. (a) COMSOL rendered depiction of electric field lines and potential drop within the three constrictive cell migration channels. (b) Bright-field image of confined channels seeding with *Dictyostelium* cells. (c) Time-lapse images of cells in the constricted channels during electrotaxis in a 2.9 V/cm strength field with the cathode to the left at the onset of the electric field (d) 3 min and (e) 6 min after the field is applied.

calls for it; for example, it can be used to easily switch between a normal buffer and a chemoattractant doped buffer for chemotaxis experiments. By maintaining flow rates/pressures equal in both sides of the device, Cell Area 7 is protected from pressure driven flows, but cells remain in a well-controlled environment that can be permeated by an electric field (for electrotaxis) or a diffusive chemical gradient (for chemotaxis) or both. As shown in Fig. 1(d), the device was composed of side flow channels ($80\,\mu$m in height) and the Cell Area 7, which was a thinner channel ($2.3\,\mu$m in height).

Cell Loading Inlet 3 was used to load cells through a restrictive serpentine channel into Cell Area 6. The cathode and anode were placed directly in contact with the buffer to produce an electric field via the locations marked Electrode Port 4 [Fig. 1(b)]. All inlets, outlets, and ports were punched out of the PDMS using a 0.75 mm biopsy punch (Ted Pella Inc.), and the electrodes used with this were 0.25 mm diameter uninsulated platinum-rhodium thermocouple wires (Omega, SPPL-010). The difference in the size of the electrodes and the biopsy punch produced electrode ports that remained open, creating a low-flow, convective waste stream on each side through which the electric field can be transmitted, but where potential redox products can be convectively prevented from reaching the cell channels. The flow rate for this convective waste stream was approximately 0.1 μl/min or 0.6% the flow rate of the main channel. This waste stream allows any Faradaic gases produced at the electrodes to be released to the atmosphere. Furthermore, reaction by-products are prevented from moving into the cell areas which would cause cell contamination and potential gradients in the pH. Therefore, although the electrodes are in direct contact with the buffer, the pressure driven flow from the inlets through the electrode channels reduces the potential for contamination and allows the device to operate without salt bridges. Moreover, although this device was used primarily at low voltages (and electric field strengths) for electrotaxis, we have tested applied voltages as high as 1000 V for periods of several hours, which create electric fields over 120 V/cm without any observable contamination. One limitation of this device, however, is that the convective waste streams will eventually overflow causing fluid to collect on top of the device. Under the above conditions, the device can run for approximately 3.5 h before the fluid should be removed. This time could easily be increased by further optimizing the flow rate, using larger biopsy punches at the electrodes to create wells with a greater volume or modifying the device to allow for drainage off the chip body.

To operate the device for studying electrotaxis, the channels were first purged using a solution of 7.5 μM cAMP in DB delivered at a pressure of 300 mbar, while the outlets, cell loading channel, and electrode ports were plugged closed. *Dictyostelium* cells excrete pulses of cAMP in their developed state and we utilized this background cAMP concentration to eliminate the possibility of cAMP-driven chemotaxis from interfering with our electrotaxis experiments. After the initial cAMP purge, *Dictyostelium* cells were loaded through the cell loading channel into the left side of the device using variable hydrostatic (gravity driven) pressure, achieved by temporarily replacing the left outlet tubing with a long length of tubing which could be manually lowered or raised to control the hydrostatic head pressure. During cell loading, the left inlet was plugged closed and the right side of the device was maintained at

atmospheric pressure. By doing this, cells were driven into the device by a slow flow and adhered to the surface at the entrances of the three confined channels, which they then invaded due to the small flow rates through the channels created by a weak pressure differential between the main loading channel and the second adjacent main flow channel. Once cells were loaded and had invaded into the confined channels, the cell loading channel was again plugged, the left outlet tubing was replaced with its standard-length tubing, and all other ports in use were unplugged. Electrodes were inserted into the channels after repurging and electric fields were then generated by applying a voltage drop across the electrodes. The device was then used to quantify cell migration behavior of Dicty as single cells traversed the length of the cell chambers. Once electrotaxis response was quantified, the ion activity in single cells was quantified by loading with an ion sensitive fluorescent indicator and observing their intracellular ion distribution. The methods, experiments, and results from these efforts—electrotaxis activity and ion activity—are presented below in Parts I and II, respectively.

PART I: ELECTROTACTIC BEHAVIOR UNDER VARIABLE DC ELECTRIC FIELD STRENGTHS
Method

To test the ability of our flow-based device for studying electrotaxis, we first performed experiments to test the ability to utilize an electric field to drive biased cell migration. After cells were loaded into the confined channels, an electric field was delivered by applying a voltage drop across the electrodes, producing a voltage drop over the path from one electrode to the other electrode, the center of this path being where the confined channels are located. This voltage drop produces a uniform electric field across the length of the microchannel. This field distribution can be modeled by solving the Laplace equation, $\nabla^2\emptyset = 0$, with constant potential boundary conditions at each end (anode-side and cathode-side) of the confinement channels. Here, the electrolyte buffer is assumed electroneutral and the variable, $\emptyset$, represents the applied potential (i.e., voltage) across the microfluidic chambers. The potential was solved numerically using a finite element package (COMSOL Multiphysics) with a triangular mesh consisting of 4482 vertices per microfluidic cell chamber. To reduce numerical error near the vicinity of the channel boundaries, the mesh element size was varied from 0.006 μm along the edges of the channel-supporting pillars and increased in size to a maximum value of 3 μm in size in the main channel domain. The electric field distribution was then computed by taking the negative gradient of the potential, $E = -\nabla\emptyset$. As shown in Fig. 2(a), the resulting electric field distribution, represented by black field streamlines superimposed atop a normalized potential distribution, is uniform across the channel length. The key result from the simulation is that the supporting channel pillars do not influence the uniformity of the electric field in the vicinity of the cell migration zones. Cells were imaged using bright-field microscopy and a 20× objective, and time-lapse micrograph videos were captured over a period of 6 minutes, as shown in Figs. 2(c)–2(e), using a Nikon Eclipse Ti microscope and a Nikon DS-Qi1Mc camera.

The cell migration was tracked by following the center mass of the cell using ImageJ (Fiji) with the MTrackJ plugin. The electrotactic

velocity was calculated by dividing the net distance the cell traveled toward the cathode (parallel to the electric field) with the total time the cell was tracked, and average speed was calculated by dividing the total distance the cell traveled in all directions by the total time the cell was tracked. Data were gathered from over 30 cells under each condition from a minimum of 3 different experiments, and results were compared using one-way ANOVA and uncorrected Fisher's LSD (least significant difference) tests with differences considered significant if P < 0.05.

Results and discussion

Our data show that the delivery of an electric field biases the direction of Dicty cellular migration toward the cathode [Fig. 3(a)].
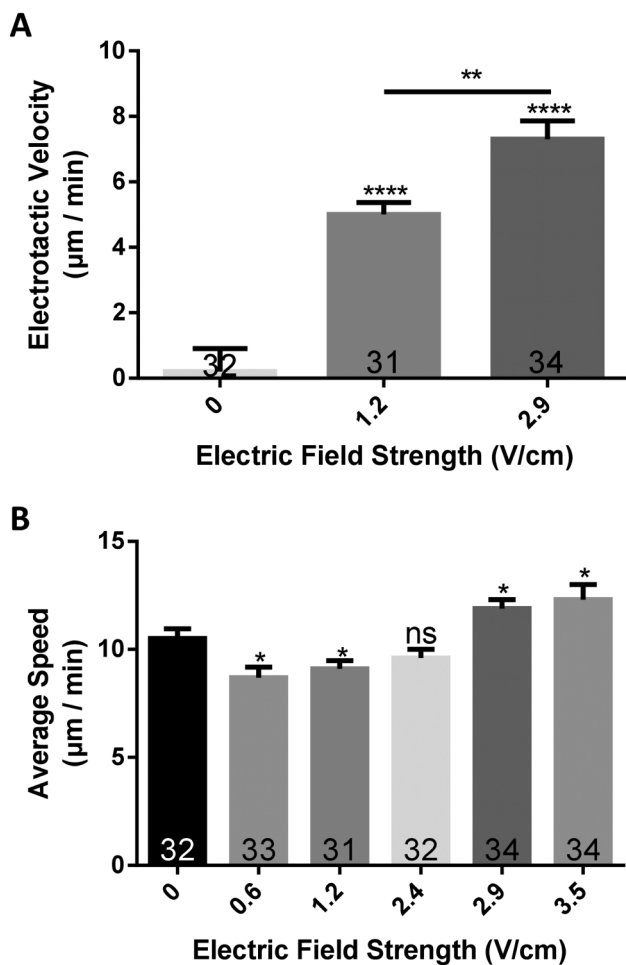
FIG. 3. (a) The electrotactic velocity (i.e., velocity of the cell in the direction of the electric field) increases with field strength and is biased in the direction of the cathode. (b) The average speed at which the cell moves is shown to be influenced by the strength of the electric field, first dropping slightly and then increasing. Cell numbers are shown on each bar, and error bars represent the standard error of the means (SEM). *P < 0.05, **P < 0.01, ****P < 0.0001.

Cells not exposed to a field had a biased electrotactic velocity of approximately $0\,\mu$m/min [Fig. 3(a)], where the horizontal component of cell velocity in cells migrating to the left was balanced by the same component of velocity in cells moving to the right. This indicates that cells did not, on average, move in a biased direction in the absence of an electrical stimulus. However, when exposed to an electric field of 1.2 V/cm, cells had an electrotactic velocity of $5.0 \pm 2.1\,\mu$m/min. Moreover, it was observed that this velocity significantly increases (P < 0.01) with electric field strength and increases to $7.3 \pm 3.2\,\mu$m/min at a field strength of 2.9 V/cm [Fig. 3(a)]. Furthermore, when outside the influence of an electric field (0 V/cm), cells tend to travel with an average speed of about $10.5 \pm 2.6\,\mu$m/min, but this average speed varies statistically (P < 0.05) with the field strength. At lower field strengths of 0.6 and 1.2 V/cm, cells move at a slower speed of 8.7 ± 2.8 to $9.1 \pm 2.1\,\mu$m/min, whereas at higher fields such as 2.9 and 3.5 V/cm cells move at a faster speed (11.9 ± 2.4 and $12.3 \pm 4.1\,\mu$m/min). It was also found that cells in a field of 2.4 V/cm, which is intermediate to the "low" and "high" fields above, exhibit no significant changes in the average speed ($9.6 \pm 2.3\,\mu$m/min) compared to cells in the absence of a field.

Combining these two results, the data showing that cells under the influence of greater field strengths move farther toward the cathode/have a greater electrotactic velocity could be because they also moved at a faster average speed. This could be because, when in the electric field, cells are observed to slowdown or stop entirely to reorient themselves to the direction of the field. In smaller field strengths, this may cause their average speed to drop. However, in larger fields, the degree to which cells are stimulated to migrate in the field direction results in a decrease in motility adjustment and leads to an increase in the overall electrotactic speed.

PART II: EFFECTS OF ELECTRIC FIELD GENERATED MIGRATION ON INTRACELLULAR Ca²⁺ LOCALIZATION

Method

After investigating the ability for the flow-based device to drive cells to repeatedly and reliably electrotax, the ability of the device to quantify ion activity in real time during migration was explored. Due to the previous work illustrating calcium's importance, we sought to use our device to investigate this ion's activity during electrotaxis migration in an electric field.

To study calcium activity and how this ion accumulates and localizes within a migrating cell, developed *Dictyostelium* cells were loaded with the fluorescent indicator of intracellular calcium Fluo 3-AM using the facilitator Pluronic F-127 (at final concentrations of $2.2\,\mu$M and 0.005 vol. %, respectively). Confocal fluorescent imaging of this indicator was performed using swept field confocal microscopy ($70\,\mu$m confocal slit, Nikon/Prairie Technologies), an Andor iXon 897 camera, a 50 mW solid state laser for excitation, and a 60× oil objective [numerical aperture 1.49]. Example resulting micrographs from this imaging are shown in Figs. 4(a) and 4(b).

To measure the relative concentration of the intracellular calcium and how this profile is influenced by the electric field, we computed an intensity ratio, calculated from the indicator intensity at the front of the cell in relationship to the back of the cell $I_{Ratio} = \frac{I_{Front}}{I_{Back}}$. The front and back of the cell were determined by the
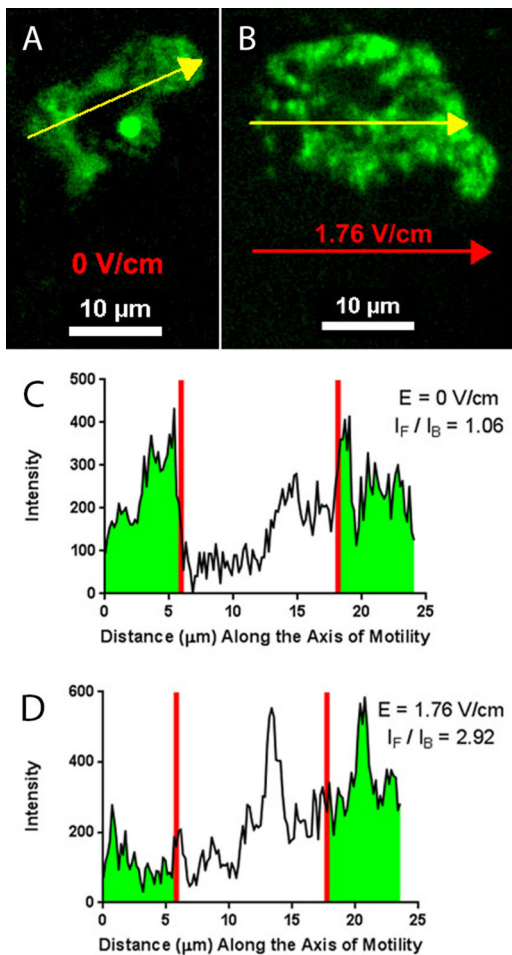
FIG. 4. (a) Confocal image of Fluo 3-AM in response to intracellular calcium in the absence of an electric field. (b) Confocal image of the localization of intracellular calcium during electrotaxis in a field strength of 1.76 V/cm. Yellow arrows indicate both the direction of cell migration and the points at which intensity values were obtained. The red arrow shows the direction of the electric field. (c) Intensity plot illustrates the values used to calculate the average intensity ratio of the front of the cell to the back of the cell. For this cell, in the absence of a field, the intensity ratio is approximately unity (1.06). (d) In a field strength of 1.76 V/cm, the intensity ratio is approximately 2.9. Red lines indicate the boundaries for which intensity measurements (highlighted green) were spatially averaged over the front and back of the cell.

direction in which the cell was moving along the axis of motility. For *Dictyostelium* cells migrating in the absence of any stimulus, this axis was taken as the direction that the cell was moving over each acquired time point. During each cell experiment, we determined the axis of motility and computed the ratio of the average calcium intensity at the leading quarter of the cell and at the trailing quarter of the cell. This measurement was performed four times for each cell at different frames in the video time lapse and then repeated for a sample size between 10 and 15 cells over a minimum of three different electrotaxis experiments. The value of

one quarter of the cell was selected because the previous work with *Dictyostelium* in our lab has shown that, when under confinement, the region under the influence of the cell cortex, which functions as a modulator of membrane behavior, is approximately one fourth of the cell's width/length.[4]

Results and discussion

Using our electrotaxis device and the experimental procedure described above, we quantitatively analyzed the intracellular calcium for cells electrotaxing in an electric field [Figs. 4(c) and 4(d)]. As a comparative experiment, we also performed this analysis for cells migrating by chemotaxis in a 20 nM/μm gradient of cAMP and for cells undergoing random walks in the absence of any stimulus (no electric field and no cAMP gradient). We observed that for both the cAMP and no stimulus experiments, the intensity ratio of the calcium indicator was very close to unity. In other words, during migration (by chemotaxis[19] and random migration), we did not observe calcium localize preferentially to a specific front or back of the cell. An electric field was then applied to observe how migration by electrotaxis would affect the local intracellular calcium concentrations.

When an electric field was applied and cells underwent electrotaxis, we observed that calcium preferentially translocated to the leading edge of the cell. This is displayed as an intensity ratio above unity and shows that the calcium concentration inside the cell is greater at the front of the cell (i.e., the side nearest the cathode), as shown in Fig. 4(d). Moreover, these data show that field strength also plays a role in dictating the magnitude of this ratio. Shown in Fig. 5, an increase in the electric field strength leads to higher
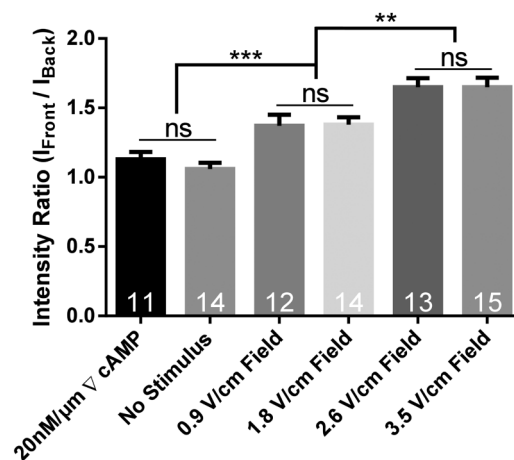
FIG. 5. Graph of intensity ratios for intracellular calcium indicator, Fluo 3-AM under different cell stimuli. Calcium remains unlocalized in the presence of a large chemoattractant gradient and in the absence of a chemical and electrical stimulus. When a field is applied, the voltage magnitude influences the relative localization of intracellular calcium for cells during electrotaxis, with calcium increasingly preferentially localizing at the front of the cell with increasing voltage. Cell numbers are shown on each bar and error bars represent the standard error of the means. **$P < 0.01$, ***$P < 0.001$.

concentrations of calcium at the front of the cell relative to the back of the cell when compared to lower field strengths (or a lack of electric field).

Our experiments illustrate that the delivery of an exogenous electric field along with the magnitude of the electric field influences the degree of localization of intracellular calcium within electrotaxing *Dictyostelium* cells. However, Ca^{2+} localization at the leading edge is not observed with cells chemotaxing up a cAMP gradient and likewise with cells undergoing migration in the absence of an external cue. Based on these results, we can speculate that the localization of calcium can play a potential role in triggering and biasing the direction of the cell motion during electrotaxis. Our results support previous data demonstrating that extracellular calcium is required for electrotaxis.[12] However, future work will leverage our ion imaging experiments with varying mutant strains of *Dictyostelium* to further elucidate the localized influence of calcium on downstream signaling pathways involved in cell motility.

CONCLUSIONS

By designing a new flow-based device with confinement chambers, our lab has created an effective tool for quantifying cell migration and intracellular ion concentrations in electric fields without salt bridges. Moreover, this tool is easy to fabricate, setup, and operate, features that can be lacking in many experimental setups for electrotaxis studies. While a commercial flow controller was used in this study, low-cost alternatives are available and easy to build in-house.[20] Using this microfluidic device, we were able to track cell migration inside confined channels and used these data to determine how electric field strength influences cell electrotactic velocity and average speed. In addition to this, we showed that our device can be used for detailed studies of intracellular mechanisms and investigated ionic calcium localization within electrotaxing cells. Finally, we demonstrated that during electrotaxis, *Dictyostelium* cells exhibit a translocation of calcium to the leading edge of the migrating cell. This phenomenon is not observed for cells migrating by chemotaxis in a cAMP gradient or for cells migrating randomly without any external cues (no field or chemical gradient). The mechanism for why intracellular calcium response is influenced by an electric field and not a chemical gradient is not well understood and will require further study. However, a device such as this platform will make an ideal experimental system for which to study electrotaxis. To further elucidate the mechanism by which cells sense and respond to electric fields, additional experiments will need to be performed, for example, investigating ion transport across the cell membrane and the effect of the external field strength on the rate of ionic flux throughout the cell during the initial onset of electrotactic migration and perhaps exposing cells to different types of electric fields, including those produced by a low frequency alternating current (AC). Finally, important downstream signaling pathways and their role in ion transport will be investigated using the library of mutant strains of Dicty available.

SUPPLEMENTARY MATERIAL

See the supplementary material for a time-lapse video of electrotaxing Dicty cells. Dicty cells loaded with Fluo 3-AM migrate directionally toward the cathode under microfluidic confinement in an externally applied electric field (1.76 V/cm).

REFERENCES

[1]A. M. Rajnicek, C. D. McCaig, B. Song, and M. Zhao, "Controlling cell behavior electrically: Current views and future potential," Physiol. Rev. **85**(3), 943–978 (2005).

[2]G. Tia, B. Reid, L. Cao, and M. Zhoa, "Electrotaxis and wound healing: Experimental methods to study electric fields as a directional signal for cell migration," Methods Mol. Biol. **571**, 77–97 (2009).

[3]R. Nuccitelli, "Endogenous electric fields in embryos during development, regeneration and wound healing," Radiat. Prot. Dosim. **106**(4), 375–383 (2003).

[4]M. Ibo, V. Srivastava, D. N. Robinson, and Z. R. Gagnon, "Cell blebbing in confined microfluidic environments," PLoS ONE **11**(10), e0163866 (2016).

[5]J. Li and F. Lin, "Microfluidic devices for studying chemotaxis and electrotaxis," Trends Cell Biol. **21**(8), 489–497 (2011).

[6]P. C. T. Chang, G. L. Sulik, H. K. Soong, and W. C. Parkinson, "Galvanotropic and galvanotaxic responses of corneal endothelial cells," J. Formos. Med. Assoc. **95**(8), 623–627 (1996).

[7]D. Wu, X. Ma, and F. Lin, "DC electric fields direct breast cancer cell migration, induce EGFR polarization, and increase the intracellular level of calcium ions," Cell Biochem. Biophys. **67**, 1115 (2013).

[8]M. B. A. Djamgox, M. Mycielska, Z. Madeja, S. P. Fraser, and W. Korohoda, "Directional movement of rat prostate cancer cells in direct-current electric field: Involvement of voltage-gated Na^+ channel activity," J. Cell Sci. **114**(14), 2697–2705 (2001).

[9]Y.-S. Sun, S.-W. Peng, and J.-Y. Cheng, "In vitro electrical-stimulated wound healing chip for studying electric field-assisted would healing process," Biomicrofluidics **6**(3), 034117 (2012).

[10]R. Gao, S. Zhao, X. Jiang, Y. Sun, S. Zhao, J. Gao, and M. Zhao, "A large scale screen reveals genes that mediate electrotaxis in *Dictyostelium discoideum*," Sci. Signal. **8**(378), ra50 (2015).

[11]Y. Li, T. Xu, X. Chen, S. Lin, M. Cho, D. Sun, and M. Yang, "Effects of direct current electric fields on lung cancer cell electrotaxis in a PMMA-based microfluidic device," Anal. Bioanal. Chem. **409**(8), 2163–2178 (2017).

[12]L. J. Shanley, P. Walczysko, M. Bain, D. J. MacEwan, and M. Zhao, "Influx of extracellular Ca^{2+} is necessary for electrotaxis in Dictyostelium," J. Cell Sci. **119**(22), 4741–4748 (2006).

[13]P. Borys, "The role of passive calcium influx through the cell membrane in galvanotaxis," Cell. Mol. Biol. Lett. **18**(2), 187–199 (2013).

[14]Y.-S. Sun, "Studying electrotaxis in microfluidic devices," Sensors **17**(9), 2048 (2017).

[15]Y.-S. Sun, S.-W. Peng, K.-H. Lin, and J.-Y. Cheng, "Electrotaxis of lung cancer cells in ordered three-dimensional scaffolds," Biomicrofluidics **6**(1), 014102 (2012).

[16]J. E. Segall and G. Gerisch, "Genetic approaches to cytoskeleton function and the control of cell motility," Curr. Opin. Cell Biol. **1**, 44–50 (1989).

[17]M. Sato, M. Ueda, H. Takagi, T. Watanabe, T. Yanagida, and M. Ueda, "Input-output relationship in galvanotactic response of Dictyostelium cells," BioSystems **88**(3), 261–272 (2007).

[18]J. Friend and L. Yeo, "Fabrication of microfluidic devices using polydimethylsiloxane," Biomicrofluidics **4**(2), 026502 (2010).

[19]S. Yumura, K. Furuya, and I. Takeuchi, "Intracellular free calcium responses during chemotaxis of Dictyostelium cells," J. Cell Sci. **109**, 2673–2678 (1996).

[20]N. Mavrogiannis, M. Ibo, X. Fu, F. Crivellari, and Z. Gagnon, "Microfluidics made easy: A robust low-cost constant pressure flow controller for engineers and cell biologists," Biomicrofluidics **10**(3), 034107 (2016).